Journal of Power Sources 265 (2014) 20–29

Contents lists available at ScienceDirect

Journal of Power Sources

journal homepage: www.elsevier.com/locate/jpowsour

Coking suppression in solid oxide fuel cells operating on ethanol by applying pyridine as fuel additive

Wei Wang [a,b], Feng Wang [a,b], Ran Ran [a,b], Hee Jung Park [d], Doh Won Jung [d], Chan Kwak [d,1], Zongping Shao [a,c,*]

[a] State Key Laboratory of Materials-Oriented Chemical Engineering, Nanjing Tech University, No. 5 Xin Mofan Road, Nanjing 210009, China
[b] College of Chemistry & Chemical Engineering, Nanjing Tech University, No. 5 Xin Mofan Road, Nanjing 210009, China
[c] College of Energy, Nanjing Tech University, No. 5 Xin Mofan Road, Nanjing 210009, China
[d] Samsung Advanced Institute of Technology (SAIT), 14-1 Nongseo-dong, Yongin-si, Gyunggi-do 446-712, Republic of Korea

HIGHLIGHTS

- The addition of pyridine could decrease the coke formation rates of Ni/Al_2O_3.
- The addition of pyridine could improve the operational stability of the fuel cells.
- Pyridine preferentially occupied the surface acidic sites of Ni/Al_2O_3.
- High power output of 1111 mW cm^{-2} was obtained with ethanol-pyridine at 750 °C.

ARTICLE INFO

Article history:
Received 6 February 2014
Received in revised form
16 April 2014
Accepted 22 April 2014
Available online 1 May 2014

Keywords:
Solid oxide fuel cells
Ethanol
Coke formation
Pyridine
Nickel–alumina

ABSTRACT

In this study, pyridine was used to suppress the coke formation in solid oxide fuel cells (SOFCs) operating on liquid fuels. Pyridine can selectively occupy acidic sites of the Ni/Al_2O_3 catalyst layer and solves the problem of dehydration of ethanol in principle, resulting in a significant reduction in the coke formation rate for operating on ethanol fuel. At 600 °C, by adding 12.5 vol.% pyridine into the ethanol fuel, the coke formation rate over the Ni/Al_2O_3 catalyst is reduced by 64% while a cell power output comparable to that operating on hydrogen is still achieved based on total potential hydrogen available from ethanol. The effective reduction of carbon deposition on the catalyst layer thus protects the anode layer from carbon deposition by strongly suppressing coke formation, especially near the anode-electrolyte interface. Pyridine is adsorbed onto the acidic sites of the Ni/Al_2O_3 catalyst and the adsorbed pyridine may reduce the amount of carbonium ions formed, thereby reducing coke formation. This study suggested that the addition of pyridine could suppress the coke formation in SOFCs with Ni/Al_2O_3 catalyst layer operated on ethanol or some other similar liquid fuels.

1. Introduction

Energy is fundamental for maintaining high quality of our life, and a sustainable supply of green energy is critical for the healthy development of our society. By considering limited resources of fossil fuels, renewable biofuels have attracted more and more attention as alternative sources of energy supply. Among them, bioethanol, which can be derived from agricultural byproducts and biomass, has been paid special importance over the past years. On the other hand, increasing the conversion efficiency during the fuel utilization is also helpful towards a sustainable future; in this regard, fuel cells represent a superior technology for generating electric power from fuels. The combination of renewable energy materials and fuel cell technology could provide a highly efficient way to create a sustainable energy supply for the future.

As high temperature electrochemical devices, solid oxide fuel cells (SOFCs) have received worldwide attention over the past decades because of their relatively low cost, improved tolerance towards impurities, and fuel flexibility [1–4]. Ethanol as a fuel for SOFCs offers the advantages of wide availability, high energy density, and convenience in handling, transportation and storage. Low-temperature SOFCs operating on ethanol fuel may serve as an

* Corresponding author. College of Energy, Nanjing Tech University, No. 5 Xin Mofan Road, Nanjing 210009, China. Tel.: +86 25 83172256; fax: +86 25 83172242.
1 Tel.: +82 31 280 6721; fax: +82 31 280 6739.
E-mail addresses: c.kwak@samsung.com (C. Kwak), shaozp@njtech.edu.cn (Z. Shao).

http://dx.doi.org/10.1016/j.jpowsour.2014.04.111
0378-7753/

alternative power source for portable applications [5–7]. Nickel cermets, which are the state-of-the-art anode materials for SOFCs, exhibit excellent activity for hydrogen electrocatalytic oxidation and high electrical conductivity; however, they also catalyze the pyrolysis of hydrocarbons and oxygenated hydrocarbons. Thus, rapid deterioration in performance often occurs when these fuel cells operate on carbon-containing fuels because of significant coke formation over the nickel anode surface. To realize the operation of SOFCs on ethanol fuel, the coking problem has to be solved.

Up to now, several attempts have been conducted to reduce the coke formation over the anode of SOFC operating on ethanol fuel, such as developing high coking-tolerant nickel-free alternative copper-ceria cermet and perovskite oxide anode materials, pre-reforming fuels to hydrogen before the fuels entering the anode chamber, and internal fuel reforming using suitable catalysts [8–11]. For internal reforming, the catalyst may be positioned near the anode surface, integrated into the fuel cells in the form of a thin film coating over the anode, or impregnated into the pore wall of the anode [10,12,13]. The fuels are converted to hydrogen and CO over the thin-film catalyst layer before they reach the anode layer, thereby increasing the power output because H_2 and CO have a higher electrochemical oxidation rate than that of most carbon-containing fuels over a nickel cermet anode. Improved operational stability is also expected due to reduced coke formation over a nickel cermet anode using reforming gas (H_2 and CO) instead of hydrocarbons and oxygenated-hydrocarbons as the direct fuel and the blocking effect of the catalyst layer for the diffusion of the primary fuel to the anode layer. There are a number of literatures concerned on the development of the coking-resistant catalysts for steam reforming of ethanol reaction and a large amount of steam as high as steam to carbon ratio of 3.0 was needed to avoid the coke formation totally [14]. However, the fuel cell could not stand for such a high content of water in the fuel since reduced overall fuel efficiency and increased internal stress will be observed with such a high steam amount. As a result, the amount of steam should be minimized in the fuel cell system.

It is well known that surface acidic sites of a catalyst usually promote the cracking reaction of hydrocarbons and consequently enhance coke formation [15]. Introducing some basic element(s), such as La, Ba, Li and Mg, into the anode could effectively decrease the amount of surface acidic sites, thereby suppressing coke formation [16–18]. The basic oxides have several effects such as it neutralizes the acidic sites which would catalyze coke deposition via the carbonium ion mechanism, and catalyzes the gasification of the adsorbed carbon deposits, thus suppress the coke formation [19]. Sometimes, such foreign elements may however significantly impact the ionic transportation properties of the electrode, thus decreasing the cell power output. The addition of a basic gas to the fuel to occupy the acidic sites of the Ni-based catalysts could be a useful way to solve the problem of coke formation. The selection of the basic gas should be carefully considered and the probes for the examination of acidic sites could be excellent additives to the fuel gas to reduce the coke formation. Infrared spectroscopy (IR) and temperature-programmed desorption (TPD) has been used extensively to measure catalyst acidity and the widely used detecting probes are ammonia and pyridine.

Recently, we developed a new and facile way of reducing coke formation rate over a conventional nickel cermet anode for methane operation by simply introducing ammonia, a basic gas, as an additive to methane [20]. Ammonia preferentially occupied the surface acidic sites of both the anode and the catalyst layers to suppress methane adsorption, thus decreasing the coke formation rate. Unfortunately, NH_3 easily decomposed in the presence of a nickel catalyst at temperature as low as 600 °C [20]. Most of the ammonia likely decomposed at the temperatures when partial oxidation or steam reforming of methane started to occur, thus reducing the efficiency of the suppression of coke formation. As a basic gas, ammonia also reacts easily with ethanol in the presence of transition metal catalysts, making the use of ammonia as an ethanol fuel additive impractical. Actually, the products for the reaction between NH_3 with ethanol at elevated temperatures are very complex, including ethylamine, diethylamine as well as the acetonitrile, which are very poisonous. Based on the thermodynamic software (HSC Chemistry ver. 5.0), the equilibrium constants of the above reactions are very large and increased with the increase in temperature (typically $\lg K > 5$ at 600 °C), suggesting the reverse reaction should be impossible to happen at above 600 °C. As a result, the combination of ethanol and ammonia are not practical.

In this study, we reported for the first time that significant improvement of coking resistance of SOFCs with conventional nickel cermet anode operating on ethanol fuel was successfully achieved by applying pyridine as a fuel additive in combination with the adoption of an anode catalyst layer, while high power output and good operational stability are obtained. It provides a novel and facile means of effectively suppressing coke formation over SOFC anodes for operation with ethanol fuel.

2. Experimental section

The fuel cell used for performance testing was in an anode substrate-supported thin-film electrolyte configuration, and an anode catalyst layer was used for improving ethanol decomposition/reforming reactivity. The anode material was a mixture of NiO + $(Y_2O_3)_{0.1}(ZrO_2)_{0.9}$ (YSZ) with a NiO to YSZ weight ratio of 60:40, prepared by physical mixing. YSZ, $Sm_{0.2}Ce_{0.8}O_2$ (SDC) and $Ba_{0.5}Sr_{0.5}Co_{0.8}Fe_{0.2}O_{3-\delta}$ (BSCF)/$Sm_{0.5}Sr_{0.5}CoO_{3-\delta}$ (SSC) composite was used as the materials of electrolyte, buffer layer and cathode, respectively. Two types of catalysts were used: a Ni/Al_2O_3 catalyst which was composed of 15 wt.% nickel with the balance being Al_2O_3, and a Li and La co-modified Ni/Al_2O_3 catalyst which was composed of 15 wt.% nickel, 1 wt.% Li_2O, 5 wt.% La_2O_3 with the balance being Al_2O_3. The catalysts were synthesized by a glycine nitrite process (GNP), which has been described in detail elsewhere [20], whereas the BSCF, SDC and SSC cathode materials were synthesized by an EDTA-citrate complexing sol–gel process [21].

Half cells of Ni-YSZ anode substrate supported thin film YSZ electrolyte with SDC buffer layer were prepared by tape-casting for the anode-YSZ dual layers and screen-printing for the buffer layer, in combination with corresponding sintering processes [20]. A mixture of BSCF/SSC + SDC (in a 7:3 weight ratio) was used for the cathode, which was screen-printed onto the central surface of the electrolyte and then fired at 1000 °C in the air for 2 h. The effective geometric surface area of the cathode was 0.48 cm^2, which was used for the calculation of cell power output. The anode surface was coated with a thin catalyst layer to enhance the ethanol reforming reaction and the catalyst layer was further sintered at 750 °C for 1 h. The current collector in the stability test was created by using a stick to draw a mesh-like morphological structure of silver paste onto the cathode surface.

Coke formation over the catalysts was investigated by first treating the catalysts in an atmosphere composed of 37.5 vol.% ethanol+62.5 vol.% helium or 37.5 vol.% ethanol+12.5 vol.% pyridine+50 vol.% helium for 30 min, then the catalysts were subjected to an oxygen temperature-programmed oxidization (O_2-TPO) analysis. The laser Raman spectra of the catalysts were obtained after treating the catalysts in ethanol-containing atmospheres for 30 min using an HR800 UV Raman microspectrometer (JOBIN YVON, France) with the green line of an argon laser ($\lambda = 514.53$ nm) as the excitation source. The morphologies of the

Ni–Al_2O_3 catalysts were observed by a field emission scanning electron microscope (FESEM, JEOL-S4800). The cross-sectional morphologies of the fuel cells were examined using a scanning electron microscope (SEM, Hitachi S-3400N) that was equipped with an EDX detector. The exhaust gas of the SOFC was analyzed online by a Varian CP-3800 gas chromatogram, which was equipped with a Hayesep Q, a Poraplot Q, a 5Å sieve molecular capillary columns, a thermal conductivity detector (TCD) for the separation and detection of H_2, O_2, CO, CO_2, N_2 and CH_4, and a flame ionization detector (FID) for the detection of the combustible substance. In the pyridine-TPD experiments, the samples were first reduced in H_2 at 750 °C for 1 h, cooled to 100 °C and exposed to 20 vol.% pyridine/He (50 mL min^{-1}) for 1 h. The sample was then purged with Ar at 100 °C for 1 h and heated at 10 °C min^{-1} to 800 °C. The pyridine concentration in the effluent gas was monitored online with a BELCAT-A apparatus equipped with an in situ TCD detector. The BET specific surface area of the catalysts was characterized by N_2 adsorption at liquid nitrogen temperature using a surface area analyzer (BELSORP II, Japan). Prior to nitrogen adsorption, the sample was degassed at 300 °C for 2.0 h to remove any physically adsorbed species. The surface area was determined from the linear portion of the BET equation.

The *I–V* polarization of the fuel cells was measured using a Keithley 2420 source meter in a 4-probe mode. During the measurement procedure, liquid ethanol and/or pyridine was vaporized using a water bath at 60 °C and introduced into the anode chamber using helium as a carrier. The flow rate of the hydrogen fuel or the helium carrier gas was maintained at 40 mL min^{-1} [STP]. The electrode polarization resistance was determined using electrochemical impedance spectroscopy (EIS) with a Solartron 1260 frequency response analyzer in combination with a Solartron 1287 potentiostat. The frequencies used for the EIS measurements ranged from 0.1 to 1000 kHz for signal amplitude of 20 mV. The exhaust gas from the single cell was fed into a Hiden QIC-20 mass spectrometer (MS) for in situ monitoring the different gases such NO_x, N_2, H_2, NH_3 CO_2 and CH_4.

3. Results and discussion

3.1. Carbon deposition

Coke formation is a serious problem for SOFCs that operate on carbon-containing fuels, and is closely related to the surface acidic sites on fuel cell materials (i.e., the anode or the integrated reforming catalyst) [17,20] that usually promoted the cracking reactions of hydrocarbons and oxygenated hydrocarbons. We previously developed a new way of reducing the rate of coke formation by introducing ammonia as an additive to methane fuel, which preferentially occupied the acidic sites of the catalyst surface, thereby reducing the coke formation rate by 55% at 700 °C [20]. However, the easy reaction with ethanol makes ammonia an impractical fuel additive to ethanol. Pyridine is a weakly alkaline compound that has been widely used as a probe molecule to study the surface acidity of many catalysts and/or supports. Pyridine is thermally fairly stable and does not exhibit significant decomposition up to 850 °C [22,23]. As a by-product of coal gasification, pyridine can also be synthesized from acetaldehyde and ammonia and is therefore widely available; in addition, pyridine is water- and ethanol- soluble and can be introduced into ethanol fuel fairly simply. Thus, pyridine may be an ideal additive to ethanol fuel for suppressing coke formation.

In a SOFC with an anode catalyst layer, most of the ethanol is converted to CO, H_2, CO_2 and H_2O before entering the anode layer. That is, the highest ethanol concentration should occur in the anode catalyst layer. Thus, reducing coke formation over the catalyst is a primary consideration in improving the operational stability. Here, we selected Ni/Al_2O_3 as a catalyst because it has been previously shown to be a highly active catalyst for ethanol steam reforming. To demonstrate the effectiveness of the use of pyridine in suppressing coke formation over the catalyst surface, the effect of pyridine to ethanol ratio on the coke formation rates of the Ni/Al_2O_3 catalysts at 600 °C is investigated. For example, for the ethanol to pyridine ratio of 3, we treated Ni/Al_2O_3 catalysts in the steams are composed of 37.5 vol.% ethanol+62.5 vol.% helium and a steam of 37.5 vol.% ethanol+12.5 vol.% pyridine+50 vol.% helium at 600 °C for 30 min, then conducted O_2-TPO analysis of the samples. The flow rate of ethanol was kept at 30 mL min^{-1} [STP]. We treated Ni/Al_2O_3 catalysts in a steam of The linear increase in temperature of the treated catalysts under a flowing oxygen atmosphere resulted in the progressive oxidization of deposited carbon over the catalyst surface to gaseous CO_2, which was monitored using an online mass spectroscopy and quantitatively determined from the integrated area of the CO_2 peak in the curve by applying pure $SrCO_3$ as an external standard substance. The coke formation rates on Ni/Al_2O_3 in the atmospheres with ethanol to pyridine ratios of 9:1, 6:1, 3:1 and 1.5:1 are studied with the results shown in Fig. 1. It suggested that the addition of pyridine could effectively reduce the coke formation on the Ni/Al_2O_3 catalysts in ethanol atmosphere. It was found that the concentration of pyridine appear a general linear in its effects on suppression in the coke formation rates until the ethanol to pyridine ratio increased to 3:1 and the excessive pyridine addition (1.5:1) almost had no effectiveness in the further suppression for the coke formation. As a result, the coke formation rates on the Ni/Al_2O_3 and Ni/LiLa–Al_2O_3 catalysts with the specific ethanol to pyridine ratio of 3:1 are also presented in Fig. 1. The introduction of 12.5 vol.% pyridine reduced the coke formation rate over Ni/Al_2O_3 by 64%, i.e., the coke formation rate in the presence of ethanol-pyridine (3:1) was approximately only 1/3 that in the presence of ethanol. In the later text of this study, "pyridine" refers to the specific 12.5 vol.% pyridine amount. We have previously shown that the coking resistance could also be improved by using NH_3 as an additive to methane due to preferential occupation of NH_3 over the acidic sites of the catalyst. The surface acidic sites could also be effectively reduced by introducing basic elements as catalyst promoters, e.g., by introducing Li and La into Ni/Al_2O_3 to produce the Ni/LiLa–Al_2O_3 catalyst. For comparison, we also tested the coke formation over a Ni/LiLa–Al_2O_3 catalyst for ethanol operation. The specific surface areas of the Ni/Al_2O_3 with Ni/LiLa–

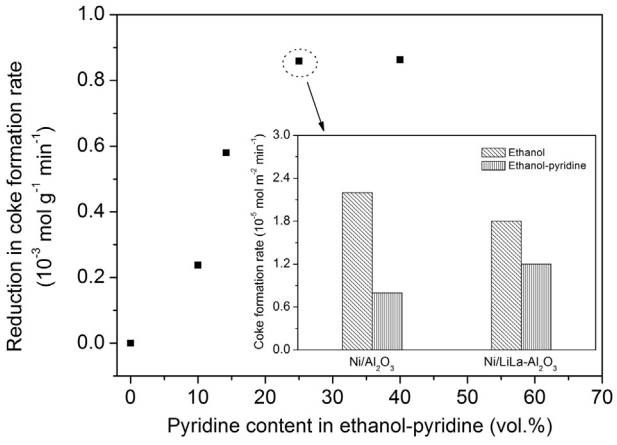

Fig. 1. Coke formation rates on Ni/Al_2O_3 and Ni/LiLa–Al_2O_3 catalysts after treatment in different ethanol-containing atmospheres for 30 min. The inlet image is the coke formation rates on Ni/Al_2O_3 and Ni/LiLa–Al_2O_3 catalysts after treatment in ethanol and ethanol-pyridine (3:1) atmospheres for 30 min.

Al_2O_3 are studied and the values are 63 and 50 $m^2\ g^{-1}$, respectively. Fig. 1 shows that the coke formation rate was 1.8×10^{-5} mol m^{-2} min^{-1} over Ni/LiLa–Al_2O_3, which was lower than that of Ni/Al_2O_3 (2.2×10^{-5} mol m^{-2} min^{-1}), as expected. Note that the subsequent introduction of pyridine reduced the coke formation rate much less significantly than that over Ni/Al_2O_3. This result can be well explained by the reduction in the number of acidic sites over Li and La oxides promoted Ni/Al_2O_3 catalyst. Surprisingly, the coke formation rate over Ni/LiLa–Al_2O_3 (1.2×10^{-5} mol m^{-2} min^{-1}) was larger than that over Ni/Al_2O_3 (8×10^{-6} mol m^{-2} min^{-1}) when pyridine was present in the ethanol. Thus, incorporating Li and La oxides into the catalyst may have created a spatial hindrance towards pyridine adsorption. It is well known that the acidic sites of Ni/Al_2O_3 catalysts are primarily Lewis acid sites, which have been identified by pyridine adsorption peaks in diffuse reflectance Fourier transform infrared spectra (DRIFTS) [24,25]. Pyridine is a strong electron donor because its lone pair of electrons on the N atom enable the Lewis acid sites to act as acceptors of H^- or e^-, thereby decreasing the positive charge of Al^{3+} and consequently reducing the number of Lewis acid sites on Al_2O_3 [26]. This mechanism may explain the suppression of coke formation on Ni/Al_2O_3 catalysts by pyridine addition to ethanol fuel. To study the behavior of pyridine adsorption on the Ni/Al_2O_3 and Ni/LiLa–Al_2O_3 catalysts, pyridine-TPD was presented and the corresponding results are shown in Fig. S2. It was found that the pyridine peak desorption with Ni/LiLa–Al_2O_3 catalyst was much lower than that of Ni/Al_2O_3, which is in good agreement with the NH_3-TPD results in our previous work, suggesting the much less acidic sites on the Ni/LiLa–Al_2O_3 catalyst [20]. On the other hand, it was found that at 600 °C, there was still a considerable amount of pyridine adsorption on the Ni/Al_2O_3 and a smaller amount at 750 °C. It suggested that the effectiveness of pyridine for the suppression of coke formation on the Ni/Al_2O_3 catalyst at 600 °C.

The nature of support strongly influences the catalytic performance of supported Ni catalyst for the steam reforming of ethanol and alumina is often used because of its mechanical and chemical

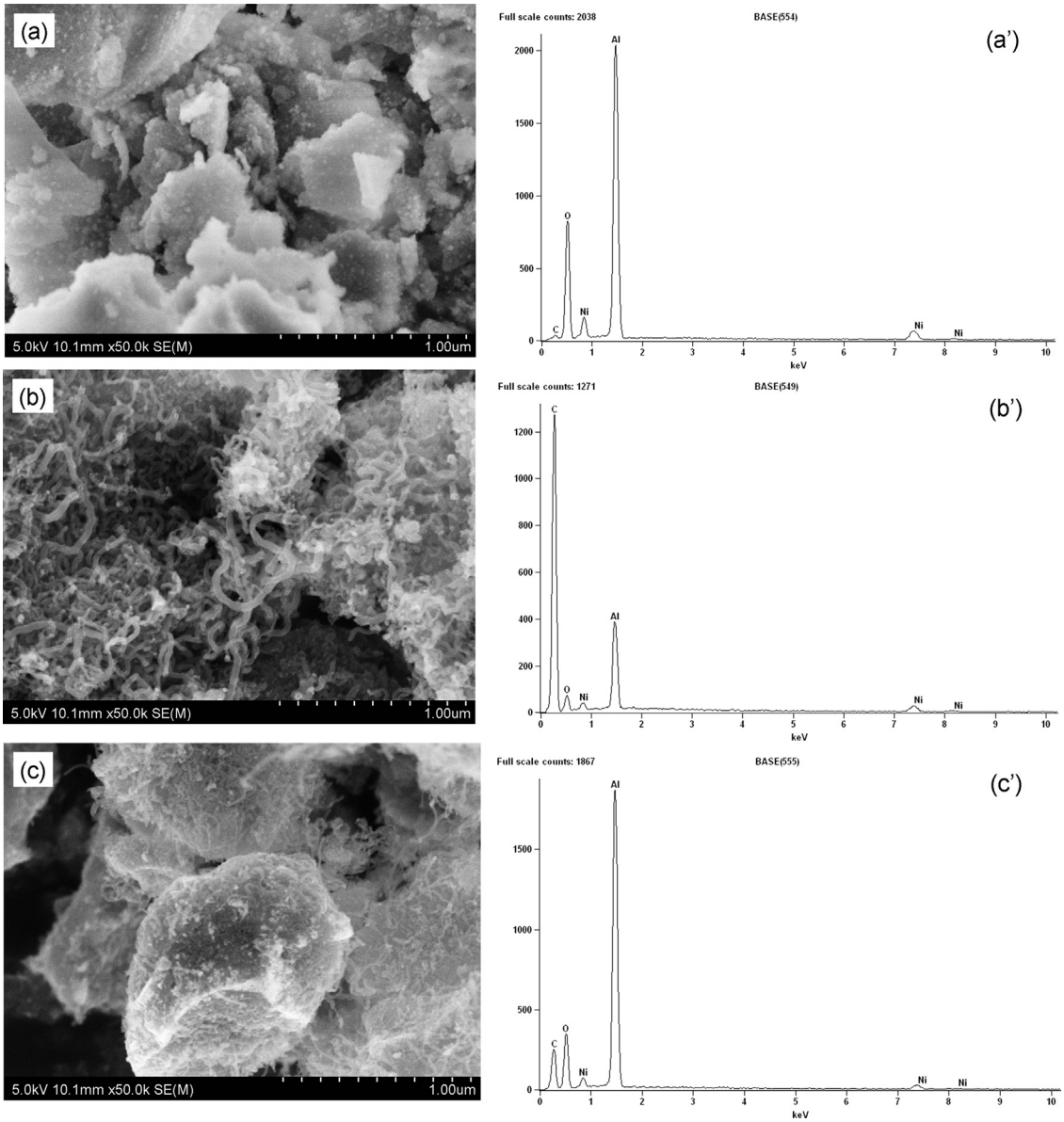

Fig. 2. SEM photos and EDX profiles of (a, a′) a fresh Ni/Al_2O_3 catalyst, (b, b′) after treatment in pure ethanol at 600 °C and (c, c′) after treatment in ethanol-pyridine at 600 °C.

resistance under the reaction conditions. The ethanol decomposition through acetaldehyde intermediate includes the following two reactions: $CH_3CH_2OH \rightarrow H_2 + CH_3CHO$, $CH_3CHO \rightarrow CH_4 + CO$ while the ethanol decomposition through ethylene intermediate includes the following two reactions: $CH_3CH_2OH \rightarrow H_2O + C_2H_4$, $C_2H_4 \rightarrow H_2 + C$. Ethanol decomposition through ethylene intermediate are prone to coke formation since olefins are highly prone to carbon formation. However, the alumina promotes carbon deposition induced catalyst deactivation from the ethylene intermediate produced via dehydration reactions of ethanol on acid sites of the support [27]. As a result, the occupation of the acidic sites on alumina by pyridine could reduce the ethylene intermediate to suppress the coke formation.

The suppression of coke formation over Ni/Al_2O_3 by introducing pyridine was more clearly demonstrated from SEM observation. Fig. 2 shows SEM images for a fresh hydrogen-reduced Ni/Al_2O_3 catalyst and Ni/Al_2O_3 catalysts that were treated in ethanol or ethanol-pyridine at 600 °C for 30 min. A large amount of filamentous carbon was observed on the catalyst after the treatment in pure ethanol (Fig. 2(b)), whereas such coke formation was substantially decreased in the presence of 12.5 vol.% pyridine under the same conditions, as indicated by the absence of these carbon fibers (Fig. 2(c)), in good agreement with the results as shown in Fig. 1. The effective suppression of carbon deposition by introducing pyridine was also quantitatively supported by the EDX analysis. Fig. 2(a′) shows that the fresh Ni/Al_2O_3 only exhibited a weak carbon peak, which could indicate carbon contamination during sample handling: the carbon content was determined to be approximately 12 wt.%. The Ni/Al_2O_3 catalyst exhibited a large carbon signal after the ethanol treatment (Fig. 2(b′)), and the carbon content reached 91 wt.%. Introducing pyridine into ethanol resulted in a carbon content of approximately 52 wt.% (Fig. 2c′), which was significantly lower than that for the catalyst that treated in ethanol.

Raman spectroscopy is a useful technique for studying the structures of carbon deposition. Fig. 3 shows the D and G bands in the Raman spectra of the Ni/Al_2O_3 catalysts treated under ethanol and ethanol-pyridine atmospheres. The degree of graphitization of carbon was closely related to the integrated intensity ratio of the D to G bands, R (I_D/I_G), and the R value decreased with the degree of graphitization [28]. The R values of the deposited carbon treated in ethanol and ethanol-pyridine were 1.31 and 1.89, respectively. The R value for graphite is typically much smaller than 1.0 [29]. A large R value corresponds to a high degree of disorder/defects in a carbon sample. The R values for the deposited carbon suggest that the addition of pyridine also effectively diminished the degree of graphitization of the carbon deposits. Coke formation is known to be a dynamic process that can be suppressed by lowering the degree of graphitization.

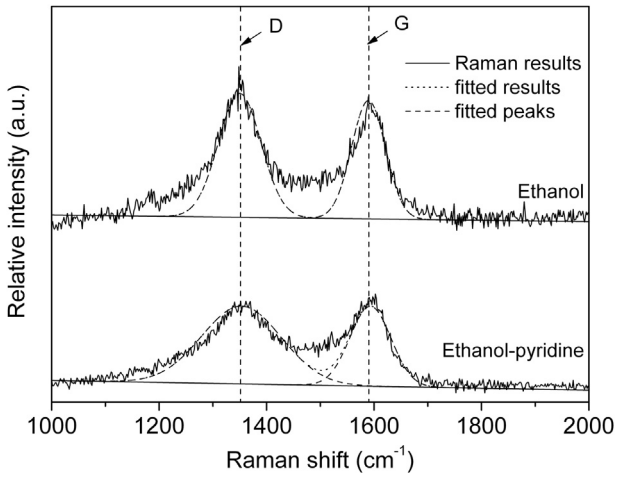

Fig. 3. Raman spectra of carbon deposited on the Ni/Al_2O_3 catalysts that were treated in ethanol or ethanol-pyridine.

3.2. Cell performance

We further tested the effectiveness of introducing pyridine for suppressing coke formation in SOFC with a conventional nickel cermet anode operating on ethanol fuel in a real single cell with the following fuel cell configuration: a Ni + YSZ anode-supported thin-film YSZ electrolyte with an SDC buffer layer and a BSCF-SDC cathode to maximize the power output. A 15 wt.% Ni/Al_2O_3 catalyst was deposited onto the anode surface to enhance the decomposition and steam reforming of ethanol to CO, H_2, CO_2 and H_2O. Fig. 4 is a representative SEM image of the cross section of the fuel cell with a reduced anode. The catalyst layer, the anode layer, the YSZ electrolyte, the SDC buffer layer and the cathode had thicknesses of approximately 30, 800, 10, 4 and 25 μm, respectively. The anode was highly porous, whereas the YSZ was well-densified without any pinholes. The pores size of the catalyst layer was much smaller pore size than that of the anode. The catalyst layer was attached fairly firmly to the anode surface, showing good compatibility between the two materials. The cathode was somewhat more densified than the anode.

Fig. 5a shows the *I–V* polarization curves at 600–750 °C for a 37.5 vol.% H_2–He fuel. A peak power density (PPD) as high as 1200 mW cm^{-2} was achieved at a cell temperature of 750 °C, and the PPD was maintained at a value of 400 mW cm^{-2} at 600 °C. The cell open circuit voltages (OCVs) were all within 1.0–1.05 V, which were slightly lower than the theoretical values because of the dilution effect of He, suggesting good densification of the electrolyte, in good agreement with the SEM observations shown in Fig. 4. This outstanding performance could be explained in terms of the thin electrolyte layer (~10 μm) and the effective elimination of the undesirable interfacial reaction between the electrolyte and the cathode by an SDC buffer layer and a high-performance cathode (BSCF + SDC). Slight concentration polarization was observed only at very high current densities (>4000 mA cm^{-2}) and elevated temperatures (700 and 750 °C), as indicated by the accelerated drop in the cell voltage with the polarization current. Thus, the catalyst layer that was deposited over the anode layer did not significantly block the gas diffusion of hydrogen. We then tested the cell for ethanol fuel operation by introducing ethanol into the fuel cell reactor as a vapor at 60 °C carried by helium at a flow rate of 50 mL min^{-1} [STP]. Under such conditions, the flow rate of gaseous ethanol was 30 mL min^{-1} [STP], and the ethanol concentration in the fuel gas was approximately 37.5 vol. %. Fig. 5b shows the *I–V* polarization curves of the fuel cells for ethanol operation at different temperatures for the initial test period. A PPD of 1100 mW cm^{-2} was achieved at 750 °C, which was just slightly lower than that (1200 mW cm^{-2}) achieved for hydrogen–helium operation at the same temperature. A PPD of 300 mW cm^{-2} was achieved even at 600 °C compared to 400 mW cm^{-2} for hydrogen operation. The aforementioned results suggest that the anode system (i.e., the catalyst and the anode layers) were also highly active in ethanol electrocatalytic oxidation. Typically, the electrocatalytic oxidation of ethanol over nickel cermet anodes primarily proceeds via an indirect route, i.e., the ethanol first decomposes to H_2, CO, H_2O and CO_2, and the CO and H_2 are then further electrooxidized to generate electricity. The cell voltages were similar to those for hydrogen fuel operation, which was a strong indicator that the ethanol oxidation occurred via this indirect route. The

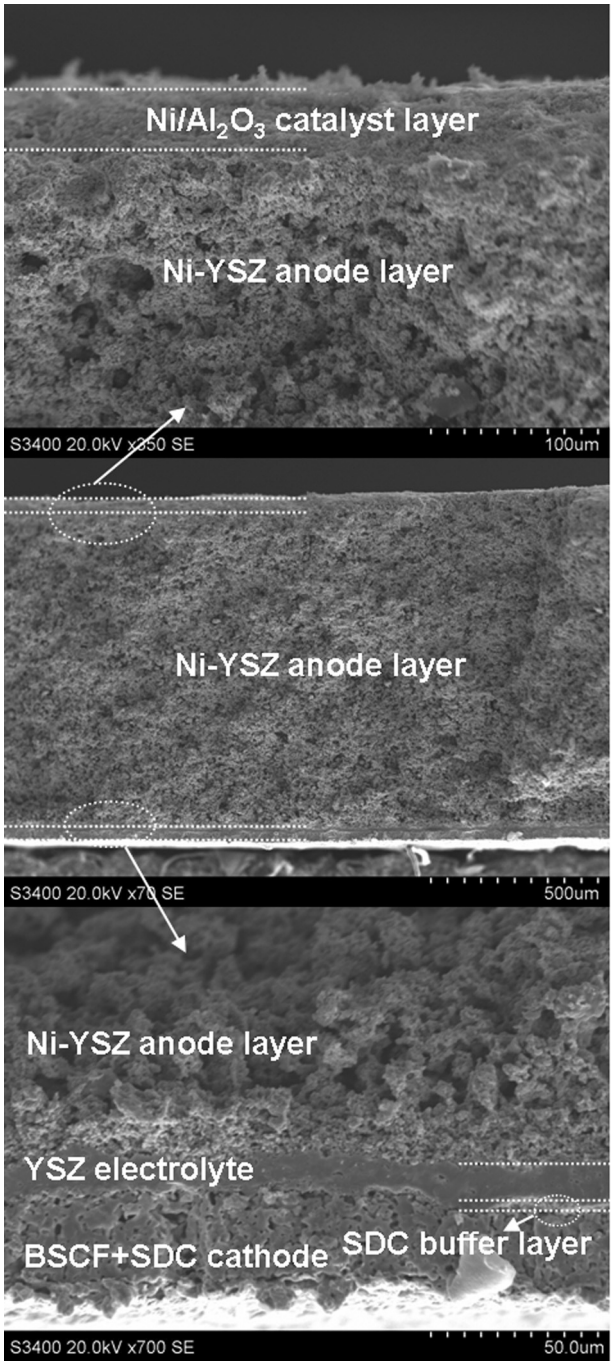

Fig. 4. A representative SEM image of a cross-section of a fuel cell with a reduced anode.

comparable cell power outputs for ethanol and hydrogen fuel operation could be explained in terms of the high activity of the catalyst layer for ethanol decomposition/steam reforming, which has already been experimentally demonstrated previously [30,31]. We chose the 90 mL min^{-1} hydrogen since it is the maximum amount of hydrogen that 30 mL min^{-1} ethanol could produce if methane could be totally converted to hydrogen. It is true that methane conversion by steam reforming is not complete and it seems impossible to generate the same amount of H_2. In addition, we found that the power outputs of the fuel cells operation on ethanol and ethanol-pyridine gas mixtures are a little lower than that of the fuel cell on 90 mL min^{-1} hydrogen and 50 mL min^{-1} He gas mixtures as the fuel shown in Fig. S1(a). It further suggested that methane was not completed converted at the fuel cell conditions, which in good agreement with the results of exhaust gas analysis of the fuel cells. Anyway, the cell performance on the ethanol and ethanol-pyridine fuels is just a little lower than that of hydrogen, suggesting the effective generation of electricity by SOFCs with ethanol and ethanol-pyridine fuels.

The effect of pyridine as an additive to ethanol fuel on the cell performance was also investigated. Fig. 5c shows the *I–V* polarization curves of the cell at different temperatures. The gas mixture was composed of helium at a flow rate of 40 mL min^{-1} [STP], gaseous ethanol at a flow rate of 30 mL min^{-1} [STP] and gaseous pyridine at a flow rate of 10 mL min^{-1} [STP]. The ethanol and pyridine concentrations in the fuel gas were controlled at approximately 37.5 vol. % and 12.5 vol.%. OCVs of 1.02–1.06 V were achieved, which were similar to those obtained for ethanol and hydrogen operation. This result suggests that pyridine addition did not affect the electro-oxidation of ethanol (in fact, H_2 and CO were the direct fuels) over the anode. Fuel utilization (U_f) is an important factor to evaluate the efficiency of electricity generation in a fuel cell by correlating the fuel consumption in quantity. To characterize the cell performance in fuel utilization, the flow rate of the two fuels was adjusted to obtain similar U_f of around 4.8% at 0.7 V and operated at 750 °C with results showing in Fig. S1(b). We found that the PPDs are 1060 and 1026 mW cm^{-2} for the ethanol and ethanol-pyridine fuels, respectively. It thus suggested that the cell with ethanol-pyridine fuel could deliver a comparable power output compared with ethanol fuel with a similar U_f. To obtain more information, we also used pyridine alone as a fuel: the corresponding *I–V* polarization curves shown in Fig. 5d. The power output of the cell was considerably reduced. A PPD of only 40 mW cm^{-2} was obtained at 600 °C. A PPD of 660 mW cm^{-2} was attained even at the highest investigated temperature of 750 °C. This observation indicated that the electro-oxidation rate of pyridine was much poorer than that of ethanol. This result is easy to understand because pyridine has been reported to have a high thermal stability up to 850 °C. Thus, the primary part of pyridine survived at 600 °C in this study. The comparable cell power output for ethanol fuel operation with and without the pyridine additive suggests that the adoption sites for pyridine and the active sites for CO/H_2 electro-oxidation on the anode layer are different.

The area-specific resistances of the fuel cell were determined from the impedance spectra. In EIS, the high-frequency offset on the real axis primarily results from the resistance of the electrolyte, whereas the difference between the high and low frequency intercepts on the real axis are associated with the electrode contribution, which includes both the anode and the cathode. The same cell was used for operation with various fuels; therefore, the difference between the electrode polarization resistances with the various fuels originated solely from the anode. Fig. 5(e) shows the impedance spectra of the fuel cell operating on various fuels at OCV conditions. The fuel cell for H_2 fuel operation exhibited the lowest electrode polarization resistance, and the fuel cell operating on pyridine fuel exhibited the largest electrode polarization resistance, in good agreement with the results shown in Fig. 5(a) and (d). The electrode polarization resistances of the fuel cells for ethanol and ethanol-pyridine operation were almost the same, in good agreement with the results shown in Fig. 5(b) and (c). The difference in the electrolyte resistances could be attributed to the different endothermic reactions that occurred in the anode chamber.

3.3. Operational stability

As previously mentioned, coke formation is a practical problem that is encountered in SOFCs with a nickel cermet anode, which may result in poor operational stability of the cell. The operational

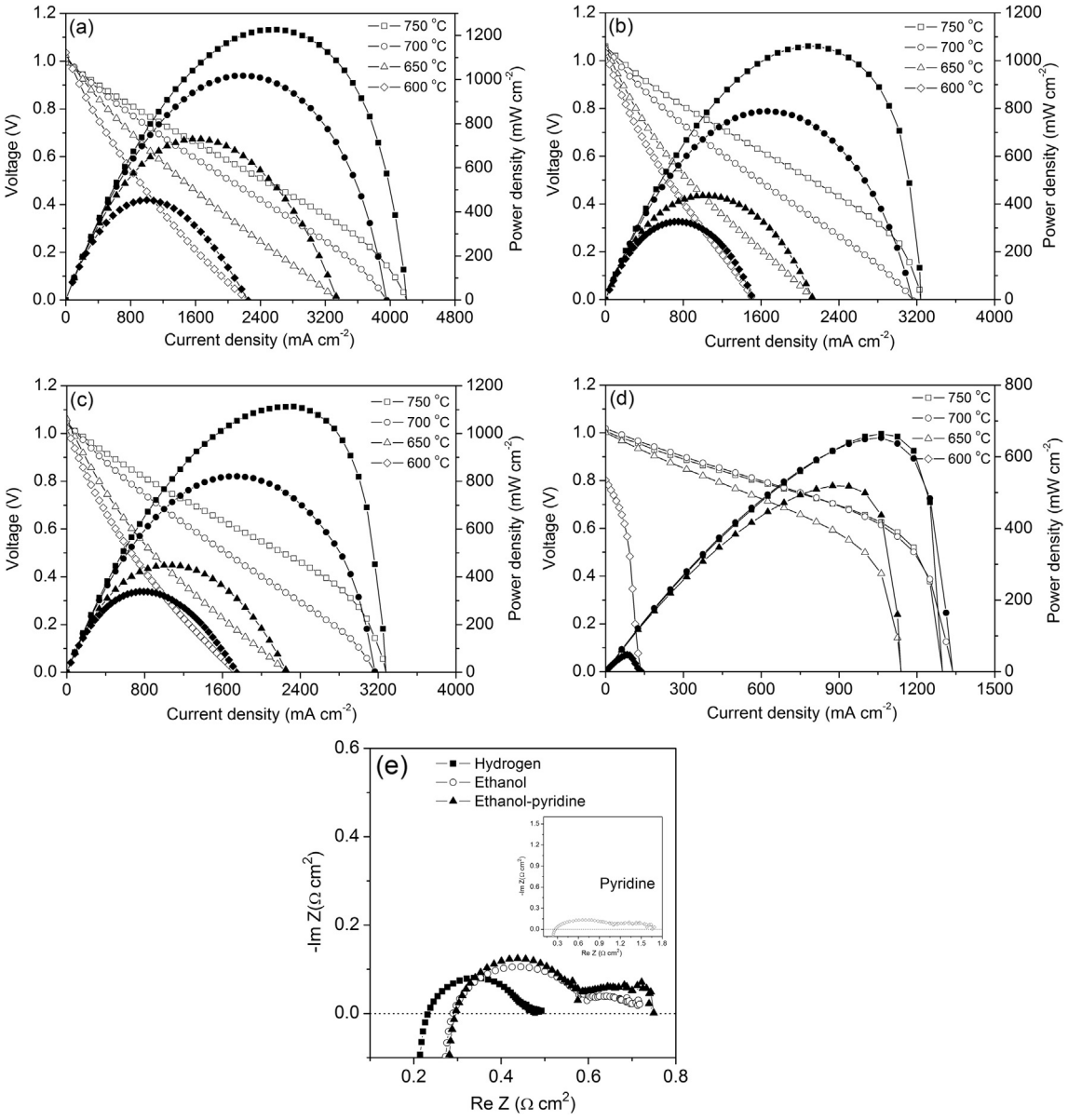

Fig. 5. *I–V* and *I–P* curves for the fuel cell operating on (a) H_2, (b) ethanol, (c) ethanol-pyridine and (d) pyridine and (e) the electrode polarization resistance of the fuel cell with different fuels at 600 °C.

stability of the current cell for ethanol fuel operation was tested under a constant current density of 150 mA cm^{-2}. To avoid potential CO_2 poisoning and a phase transition at the BSCF cathode, we used SSC as the cathode material for the stability test. Fig. 6 shows the time-dependence of the cell voltage in the operational stability. The fuel cell performance was first stabilized by polarization under a constant current density of 200 mA cm^{-2} for 24 h using hydrogen at 600 °C. Although a very high power output was initially observed, the cell performance for ethanol fuel operation was unfortunately unstable. The cell voltage initially increased slightly and reached a maximum of 0.73 V at approximately 1.8 h, followed by a sharp decrease to zero at 2.5 h. In contrast, the cell operation was stable for approximately 100 h when pyridine was added to the ethanol fuel gas. This remarkable improvement in the operational stability could clearly be attributed to the high suppression of coke formation. After de-assembling the fuel cell, we observed obvious cracks in the fuel cells and considerable coke formation over the catalyst surface for the cell with ethanol operation, as shown in Fig. S3(a). Furthermore, this fuel cell did not retain its integrity after the stability test. The aforementioned analysis shows that the Ni/Al_2O_3 catalyst was prone to coke formation for ethanol fuel operation. In contrast, Fig. S3(b) shows that the cell that operated on ethanol-pyridine gas mixtures retained its integrity very well, and no obvious carbon deposit on the catalyst surface was observed.

Following the operational stability test, the cell was subjected to SEM-EDX characterization. In this experiment, we mainly focused on the coke formation at the anode and the anode catalyst layers, i.e., the microstructure of the cathode was not considered. Fig. 7(a) shows the SEM image of a sectional view of the fuel cell. Following ethanol-pyridine operation, the cell exhibited good geometric integrity, and no delamination of the catalyst layer from the anode or of the anode layer from the electrolyte was observed. Some cracks were observed between the anode layer and the catalyst layer on the fuel cell after ethanol operation, as shown in Fig. 7(c). Fig. S4 shows the interface between the anode layer and catalyst

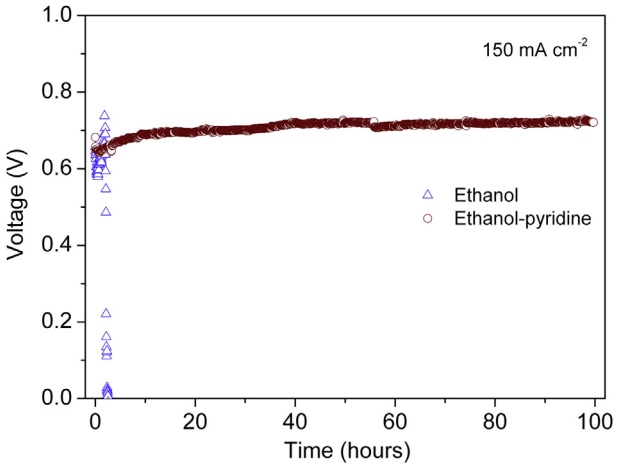

Fig. 6. Time-dependent voltage of the fuel cell operating on ethanol with and without pyridine addition under a current density of 150 mA cm^{-2} at 600 °C.

layer in detail. Fig. 7(a) shows the different zones of the two fuel cells: 1) the middle of the catalyst, 2) the middle of the anode layer, 3) the anode near the electrolyte interface and 4) the middle of the electrolyte layer. Fig. 7(b) shows the results of analyzing these zones using EDX to investigate carbon deposition. A small carbon signal was detected in the EDX micrograph of the electrolyte. The carbon content of the electrolyte layer was calculated to be approximately 8 wt.%. No carbon should have been present in the dense electrolyte layer; therefore, this carbon was most likely caused by contamination during sample handling. The carbon content in the zone near the electrolyte interface was approximately 8.3 wt.%, which was similar to that in the electrolyte, indicating that coke formation was negligible in the zone near the electrolyte where the most of the electro-oxidation of the fuels (H_2 and CO) occurred. However, the cell with a Ni/Al_2O_3 catalyst layer for ethanol fuel operation had a carbon content in zone 4′ near the electrolyte interface of approximately 16 wt.%, which was much higher than the amount of carbon in the electrolyte. Carbon deposition in the anode region near the anode-electrolyte interface would have reduced the number of active sites for the electrochemical oxidation of the fuel and resulted in significant deterioration of the cell performance, which may explain the rapid deterioration of the cell performance for ethanol operation. The highest amount of carbon deposits was found on the catalyst layer, as expected, and the lowest carbon content was found in the anode region near the anode-electrolyte interface. However, we found much higher carbon contents in zones 1′, 2′ and 3′ of the fuel cells for ethanol operation than in the corresponding regions of the cell for ethanol-pyridine operation (see Fig. 7(b) and (d)). For example, the carbon content in zone 1 was 36 wt.% compared to 64 wt.% in zone 1′. The aforementioned results strongly indicate that pyridine was effective in suppressing coking. For fuel cells under polarization condition, oxygen in the form of O^{2-} transports from the cathode to the anode and then reacted with the fuel. The flux of O^{2-} across the electrolyte from the cathode to the anode increases with the increase in the polarization current. However, the conversion of carbonaceous species, into CO, CO_2, H_2, and H_2O has also been shown to increase with the polarization current, which implies that the partial oxidation or steam/CO_2 reforming of hydrocarbons occurs over the anode during the current polarization. In this study, the clearly difference in the performance of the catalyst by itself and under SOFC operation in ethanol-pyridine atmosphere could be attributed to the existence of current density. However, under the same current density, the coke formation on the Ni/Al_2O_3 catalyst could not be eliminated without the addition of pyridine. It suggested that pyridine was very useful for the suppression of coking on the Ni/Al_2O_3 catalyst in ethanol, especially in the SOFC operation conditions.

As shown in Fig. 8, for the SOFC containing a Ni/Al_2O_3 anode catalyst layer, the fuel gas (ethanol) first passed through the catalyst layer and then underwent catalytic decomposition to form gaseous

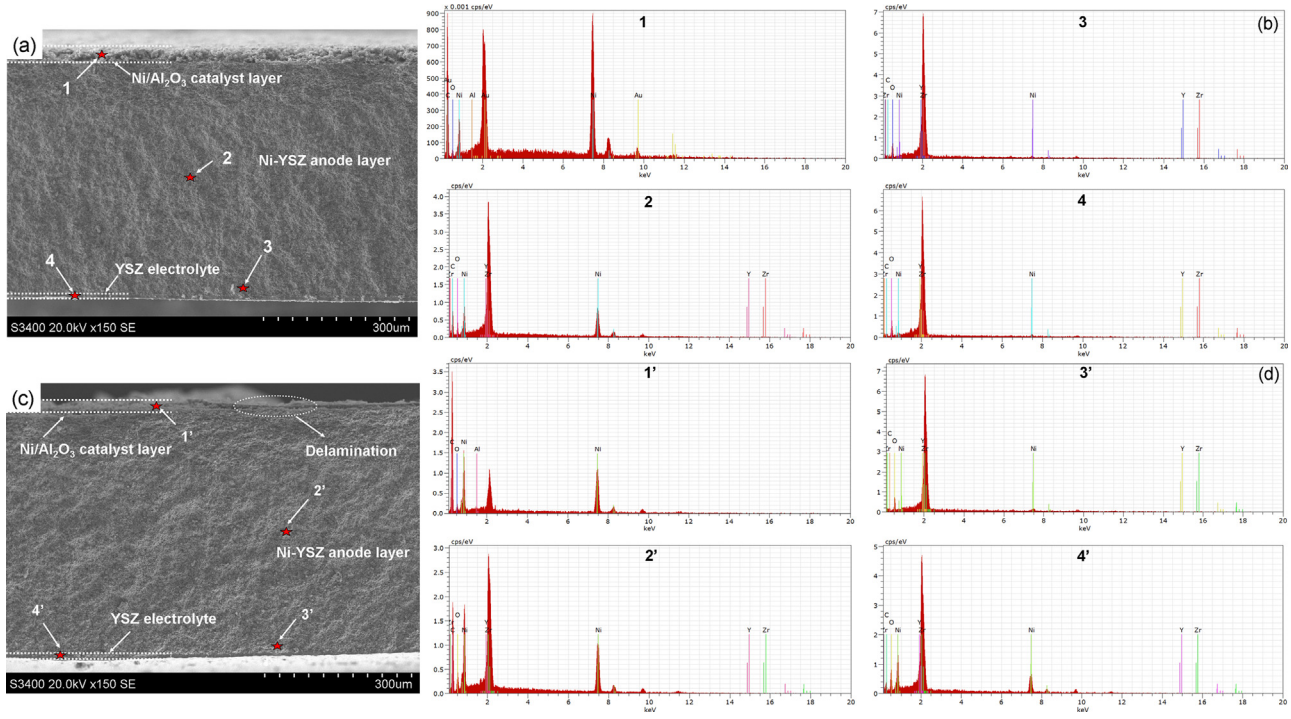

Fig. 7. SEM photos and EDX profiles of the two fuel cells following an operational stability test.

H_2, CO and solid carbon. H_2 and CO then diffused to the anode layer, where they were electro-oxidized to generate electricity and formed deep oxidation products of CO_2 and H_2O. The as-formed CO_2 and H_2O diffused outwards and passed through the catalyst layer, before finally releasing into the anode chamber as a gaseous effluent. Both deep electrochemical oxidation products of CO_2 and H_2O came into contact with the ethanol fuel in the catalyst layer, where the high activity of Ni/Al_2O_3 for ethanol steam reforming further promoted the conversion of ethanol to CO and H_2 to minimize the ethanol concentration in the catalyst layer, maximize the H_2 concentration the anode layer, and minimize the carbon deposition in the anode zone near the electrolyte interface. Therefore, maximum and minimum coke formation was observed in the catalyst layer and the anode layer near the electrolyte interface, respectively. Fig. 8 also shows the proposed mechanism for the suppression of coke formation by pyridine addition. Surface acidity is important to coking because of its effect on carbonium ions, which are important intermediates in the coke formation process [26,32,33]. Coke is believed to be formed via a mechanism involving carbonium ions: the higher the surface acidity, the greater is the carbonium ion production [34] and thus, the larger the amount of deposited carbon. The details of coke-forming reactions vary with the gas mixture of the reaction, the operating conditions and the selection of the catalysts, however, for all the conditions, it could be speculated that the reactive intermediates combine, rearrange and dehydrogenate into coke-type structures via carbonium ions-type reactions [19]. Carbonium ions could also crack to form small fragments which could further participate in the coke-forming process as hydrogen transfer agents. In this study, the relatively high thermal stability of pyridine could maximize its adsorption on the acidic sites of the Ni/Al_2O_3 catalyst, thus reducing the amount of carbonium ions formed and minimized coke formation.

To confirm the mechanism of the suppression of coke formation with pyridine addition, the exhaust gas of the same single cell operating on the ethanol and ethanol-pyridine gas mixtures was monitored by an online gas chromatogram. Shown in Fig. 9 are the selectivities of the carbon-containing products under different polarization current densities. Ethanol was totally converted under the fuel cell conditions. As can be seen, when pyridine was added to the fuel, the CO_2 selectivity increased and CH_4 and CO selectivities decreased under both OCV and polarization conditions. The increase in amount of CO_2 with the addition of pyridine suggests that the carbonium ions were preferred to be electrochemically oxidized to CO_2 instead of absorbed on the surface of the Ni/Al_2O_3 catalyst after the introduction of pyridine. Above results further confirmed the mechanism of the suppression of coke formation with pyridine addition, as shown in Fig. 8.

To investigate the possible formation of NO_x or NH_3 when pyridine was introduced into ethanol fuel gas, the exhaust gas of an SOFC operating on the ethanol-pyridine gas mixtures was also monitored by an online mass spectrometer. It was found the concentration of NO_x and NH_3 is four to five orders of magnitude lower than that of H_2, suggesting that the yield of NO_x and NH_3 is negligible. As shown in Fig. 10, no change in the absolute intensity of the NO_x and NH_3 signals was observed when the atmosphere was switched from air to the exhaust gas of the SOFC under a certain polarization current of 150 mA cm^{-2}. We have also found that the main products emissions arising from pyridine are N_2 while NH_3

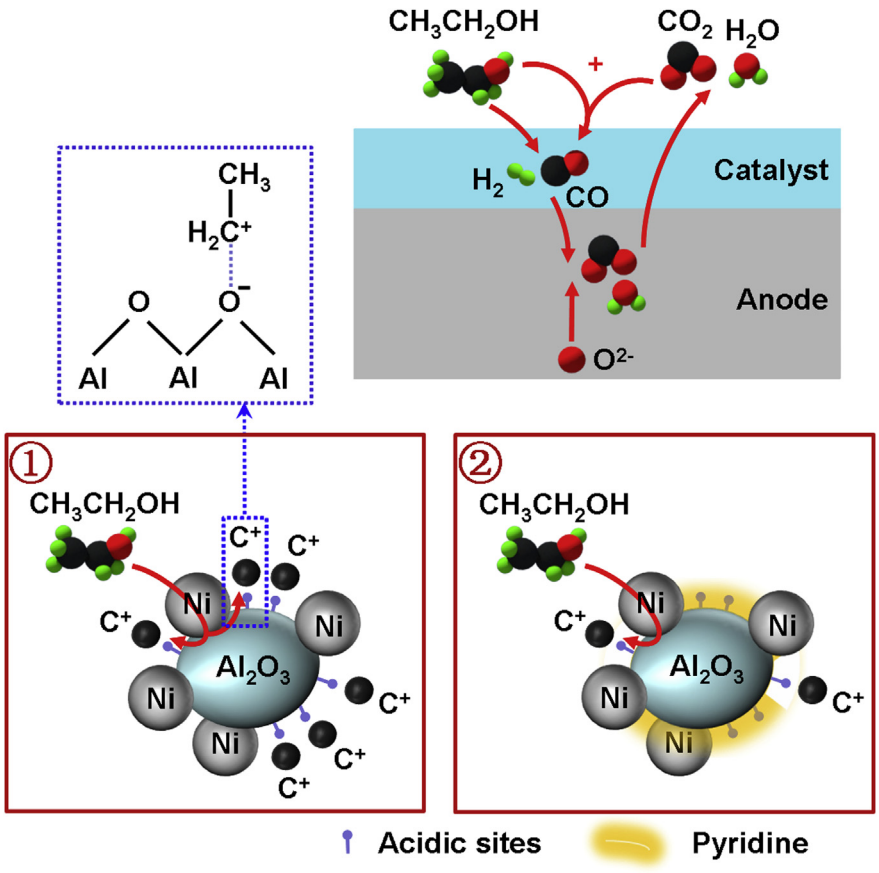

Fig. 8. Schematic of a SOFC with a catalyst layer during operation on ethanol fuel gas and the proposed mechanism for pyridine-mediated suppression of coke formation on a Ni/Al_2O_3 catalyst.

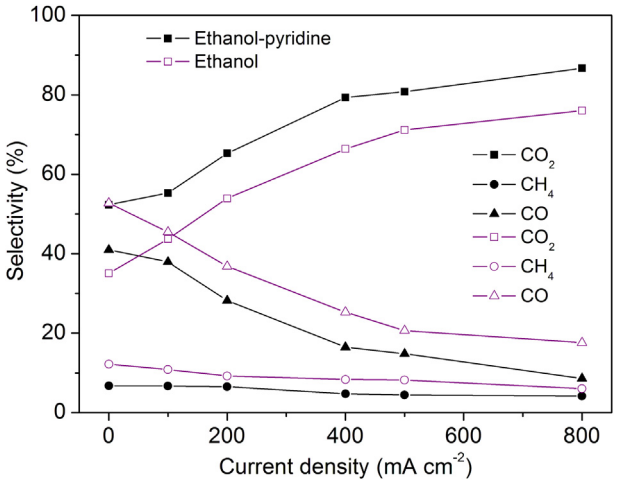

Fig. 9. The exhaust gas of the fuel cell with the Ni/Al_2O_3 catalyst layer operating on ethanol or ethanol-pyridine (3:1) gas mixtures under different current densities.

was reformed to H_2 and N_2 under the catalysis of Ni-based catalysts. The conversion of pyridine was based on the N element balance. It was found that pyridine conversions are around 10 and 11% for the fuel cell without and with the current density, suggesting that the current density could slightly improve the pyridine conversion reaction. A large amount of pyridine (as high as 90%) was remained in the emissions. An HCl solution was used to absorb the remained pyridine to form the pyridinium chloride, which is an important intermediate pharmaceutical and biochemical researches, organic synthesis as well as a raw material for methyl erythromycin production. The high quality of heat energy produced by SOFCs could be used to decompose pyridinium chloride to hydrogen chloride gas and pyridine, suggesting a regeneration process for the pyridine. On the other hand, a physical condensation method could also be used to regenerate pyridine since pyridine was the only liquid phase at room temperature in the exhaust gas based on our results in this study. As a result, pyridine could also regenerated by the condensation method.

4. Conclusions

In conclusion, we have successfully reported the suppression of coke formation by pyridine addition to ethanol fuel gas.

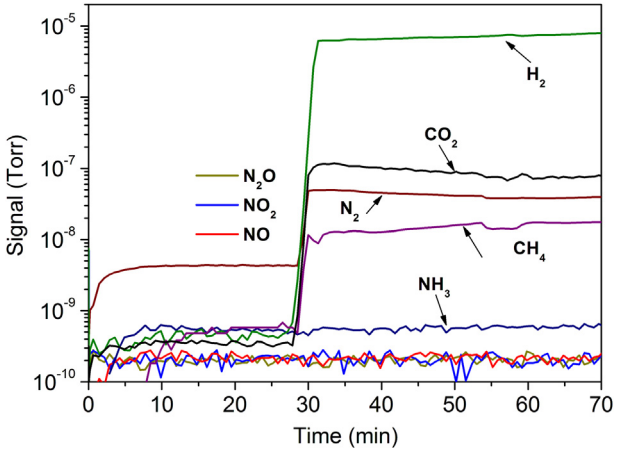

Fig. 10. The exhaust gas of the fuel cell with the Ni/Al_2O_3 catalyst layer operating on ethanol-pyridine (3:1) gas mixtures under a certain current density of 150 mA cm^{-2}.

Pyridine addition effectively improved the operational stability of cells using ethanol fuel at intermediate temperatures by suppressing coke formation on the anode catalyst layer and the anode layer, especially in the anode region near the anode-electrolyte interface. The SOFCs used in this paper can be easily fabricated using cost-effective methods and materials. This study suggested that pyridine was useful for suppressing the coke formation in the ethanol fueled SOFCs with Ni/Al_2O_3 anode catalyst layer.

Acknowledgments

This work was supported by the Samsung Advanced Institute of Technology project. Prof. Shao also acknowledges the financial support via program of "National Science Foundation for Distinguished Young Scholars of China" under contract No. 51025209.

Appendix A. Supplementary data

Supplementary data related to this article can be found at http://dx.doi.org/10.1016/j.jpowsour.2014.04.111.

References

[1] S. Park, J.M. Vohs, R.J. Gorte, Nature 404 (2000) 265–267.
[2] T. Hibino, A. Hashimoto, T. Inoue, J. Tokuno, S. Yoshida, M. Sano, Science 288 (2000) 2031–2033.
[3] Z.P. Shao, C.M. Zhang, W. Wang, C. Su, W. Zhou, Z.H. Zhu, H.J. Park, C. Kwak, Angew. Chem. Int. Ed. 50 (2011) 1792–1797.
[4] W. Wang, C. Su, Y.Z. Wu, R. Ran, Z.P. Shao, Chem. Rev. 113 (2013) 8104–8151.
[5] Y. Jiang, A.V. Virkar, J. Electrochem. Soc. 148 (2001) A706–A709.
[6] B. Huang, S.R. Wang, R.Z. Liu, T.L. Wen, J. Power Sources 167 (2007) 288–294.
[7] M.D. Mat, X. Liu, Z. Zhu, B. Zhu, Int. J. Hydrogen Energy 32 (2007) 796–801.
[8] H. Kim, C. Lu, W.L. Worrell, J.M. Vohs, R.J. Gorte, J. Electrochem. Soc. 149 (2002) A247–A250.
[9] Y.H. Huang, R.I. Dass, Z.L. Xing, J.B. Goodenough, Science 312 (2006) 254–257.
[10] W. Sangtongkitcharoen, S. Assabumrungrat, V. Pavarajarn, N. Laosiripojana, P. Praserthdam, J. Power Sources 142 (2005) 75–80.
[11] Z.L. Zhan, S.A. Barnett, Science 308 (2005) 844–847.
[12] M.M. Liao, W. Wang, R. Ran, Z.P. Shao, J. Power Sources 196 (2011) 6177–6185.
[13] S.P. Yoon, J. Han, S.W. Nam, T.-H. Lim, S.-A. Hong, J. Power Sources 136 (2004) 30–36.
[14] I. Rossetti, C. Biffi, C.L. Bianchi, V. Nichele, M. Signoretto, F. Menegazzo, E. Finocchio, G. Ramis, A. Di Michele, Appl. Catal. B Environ. 117–118 (2012) 384–396.
[15] J.J. Guo, H. Lou, L.Y. Mo, X.M. Zheng, J. Mol. Catal. A Chem. 316 (2010) 1–7.
[16] Q. Miao, G.X. Xiong, S. Sheng, W. Cui, L. Xu, X. Guo, Appl. Catal. A Gen. 154 (1997) 17–27.
[17] L. Yang, Y.M. Choi, W. Qin, H. Chen, K. Blinn, M. Liu, P. Liu, J. Bai, T.A. Tyson, M.L. Liu, Nat. Commun. 2 (2011) 357.
[18] L. Xu, H. Song, L. Chou, Appl. Catal. B Environ. 108–109 (2011) 177–190.
[19] P. Forzatti, L. Lietti, Catal. Today 52 (1999) 165–181.
[20] W. Wang, R. Ran, C. Su, Y.M. Guo, D. Farrusseng, Z.P. Shao, J. Power Sources 240 (2013) 232–240.
[21] H.X. Gu, R. Ran, W. Zhou, Z.P. Shao, J. Power Sources 172 (2007) 704–712.
[22] J.C. Mackie, M.B. Colket, P.F. Nelson, J. Phys. Chem. 94 (1990) 4099–4106.
[23] H.U.R. Memon, K.D. Bartle, J.M. Taylor, A. Williams, Int. J. Energy Res. 24 (2000) 1141–1159.
[24] X. Wang, U.S. Ozkan, J. Mol. Catal. A Chem. 232 (2005) 101–112.
[25] B.T. Loveless, A. Gyanani, D.S. Muggli, Appl. Catal. B Environ. 84 (2008) 591–597.
[26] A. Coma, Chem. Rev. 95 (1995) 559–614.
[27] S. Roy, G. Mpourmpakis, D. Hong, D.G. Vlachos, A. Bhan, R.J. Gorte, ACS Catal. 2 (2012) 1846–1853.
[28] F. Tuinstra, J.L. Koenig, J. Chem. Phys. 53 (1970) 1126–1130.
[29] D. Goers, H. Buqa, L. Hardwick, A. Würsig, P. Novák, Ionics 9 (2003) 258–265.
[30] J. Comas, F. Mariño, M. Laborde, N. Amadeo, Chem. Eng. J. 98 (2004) 61–68.
[31] G. Wang, H. Wang, Z. Tang, W. Li, J. Bai, Appl. Catal. B Environ. 88 (2009) 142–151.
[32] M. Boronat, A. Corma, Appl. Catal. A Gen. 336 (2008) 2–10.
[33] J.W. Hightower, W.K. Hall, J. Am. Chem. Soc. 90 (1968) 851–858.
[34] C.W. Fitz, H.F. Rase, Ind. Eng. Chem. Prod. Res. Dev. 22 (1983) 40–44.